Manufacturing Rev. **11**, 9 (2024)

https://doi.org/10.1051/mfreview/2024007

Manufacturing Review
Available online at:
https://mfr.edp-open.org

RESEARCH ARTICLE OPEN ACCESS

On the influence of compositional variations in high chrome cast iron: an assessment of microstructure and mechanical behaviour

Brayner Ndivhuwo Nelwalani[1,2], Josias van der Merwe[1], Vhonani Munyangane[1], Zaynab Adam Cader[1,*], Thato Rampaku[1], and Desmond Klenam[1]

[1] School of Chemical and Metallurgical Engineering, University of the Witwatersrand, Johannesburg 2050, South Africa
[2] Department of Metallurgy, School of Mining, Metallurgy and Chemical Engineering, Faculty of Engineering and Built Environment, University of Johannesburg (Doorfontein Campus), Johannesburg 2001, South Africa

Received: 31 July 2023 / Accepted: 28 February 2024

Abstract. In this study, the influence of compositional variation on the microstructure and properties of high chrome cast iron produced in jobbing foundries was evaluated. The aim was to determine whether compositional analysis alone is sufficient for qualifying acceptable high chrome cast iron components made in jobbing foundries. The compositions of the melts were analysed using optical emission spectroscopy. They were then compared with targeted compositions for commercially acceptable high chrome cast iron components. Equilibrium phases and phase transition temperatures of the different high chrome cast iron were calculated using the measured compositions as input on Thermo-Calc. Thermal analyses were also carried out to obtain the cooling profiles of each melt using ATAS MetStar software. The predictions from Thermo-Calc and ATAS Metster thermal analyses were then compared with experimentally determined optical and scanning electron images of the alloys. Hardness, fracture toughness, and wear resistance were determined both in the as-cast and heat-treated conditions. The results showed that even slight compositional variations significantly influence the microstructure and mechanical properties of high chrome cast iron, even when the compositions fall within the targeted compositional range typically accepted for industrial applications. Therefore, the study suggests that using compositional analysis alone is not sufficient for accepting high-quality high chrome cast iron components for industrial applications.

Keywords: High chrome cast iron / thermal analysis / wear / microstructure

1 Introduction

Cast irons can generally be described as ferrous alloys containing carbon content of ≥2.11 wt.%. They are typically classified into five basic types based on by their graphite morphology [1]. This includes grey cast iron which has graphite in the form of flakes, ductile or nodular cast iron with graphite present in globular form, malleable cast iron which has graphite present in the form of nuggets, compacted graphite iron with graphite shape resembling corals, and white cast iron which instead of graphite, contains metastable cementite [1]. Of interest in this paper is white cast iron (WCIs) which is known to have carbide stabilising elements like Cr, Mo and Ni. These elements are mainly responsible for the uniqueness of white cast iron as it is the only cast iron in which carbon is present as carbides [2,3]. The microstructure of white cast iron mainly consists of pearlite and cementite which are responsible for their inherent attractive properties such as high hardness, good abrasion resistance and high compressive strength. However, these attractive properties are obtained at the expense of ductility, impact toughness and fracture toughness. White cast iron is very brittle due to the absence of graphite; hence cracks can easily propagate once initiated under loading conditions [4]. White cast iron can be classified into three groups which are normal white cast iron (NWCI) containing C, Si, Mn, P and S with no other alloying elements, low alloy white cast iron (LAWCI) which has its mass fraction of alloying elements totalling less than 5% and high alloy white cast iron (HAWCI) with the alloying element mass fraction totalling to more than 5% [5].

High chrome cast iron (HCCI) is a type of HAWCIs which contain 11–30 wt.% Cr content and 1.8–3.6 wt.% C along with other alloying elements such as Si, Cu, V, Mn,

* e-mail: zaynab.cader@students.wits.ac.za

Table 1. Composition of high chrome cast iron.

HCCI	Cr	C	Si	Mn	Fe	V	Ni	Cu	Mo	Cr/C	Total percentage carbide (%)
A	22.44	2.34	0.73	1.25	72.20	0.11	0.29	0.12	0.25	10.01	25.90
B	24.04	2.40	0.65	0.78	70.90	0.13	0.31	0.16	0.28	10.79	27.50
C	22.34	2.07	0.64	0.88	73.40	0.04	0.19	0.04	0.94	9.59	22.60
D	23.90	2.40	0.67	0.78	71.00	0.13	0.31	0.16	0.29	9.95	27.50

Mo, and Ni, to impart high hardness and wear resistance in the material [6]. This cast iron is applied in applications that require high wear and corrosion resistance such as in ball mill liners, grinding rolls and slurry pumps used in the mining and mineral processing industries [4–6]. HCCI could be of hypoeutectic composition which solidifies in the hypoeutectic domain to yield a final microstructure containing primary carbides of the M_7C_3 type + ledeburite in an austenite matrix. It could also solidify as eutectic yielding a final microstructure consisting of eutectic carbides in an austenitic matrix [7]. Similar to other WCIs, the high corrosion and wear resistance of HCCI is heavily let down by poor ductility and toughness. Consequently, the use of HCCI is limited since failure of components made from HCCI can be insidious and sudden. To enhance the performance of HCCI and their use for a wider spectrum of applications, it is important to understand the relationship between their compositions, microstructures, and properties.

Abdel-Aziz et al. [8] among other researchers [2,9] shown that the microstructure and properties of HCCI can be enhanced through addition of alloying elements and heat treatment. These processes determine the size, type and morphology of carbides that largely control the performance of HCCI components in service.

In this study, the influence of compositional variations on the microstructure and properties of HCCIs produced in jobbing foundry was evaluated. This study is important given that most jobbing foundries accept HCCI casts that fall within specific compositional range as good quality. However, having castings that fall within targeted compositional range may not necessarily display comparable properties because the variations in Cr/C ratios and other alloying content may significantly affect their performance in service. This study is therefore establishing to what extent compositional variations influence the microstructure and properties of HCCIs. The outcome of this study will serve as a basis for future compositional modifications for enhanced microstructure and properties, particularly achieving good combination of surface properties, hardness, and toughness in HCCI.

2 Materials and methods

2.1 Materials

HCCIs having different compositions are presented in Table 1. The HCCI were produced in a jobbing foundry in Johannesburg, South Africa. They were compositions extracted from melts of components which targets specific range of compositions. The Cr/C ratio and total carbide volume (equation 1) were calculated in accordance with Abdel-Aziz et al. [8]

$$\text{Total\%carbides} = 12.3 \times \%\text{C} + 0.55 \times \%\text{Cr} - 15.2. \quad (1)$$

2.2 Experimental procedure

2.2.1 Thermo-Calc and ATAS simulation

Themo-Calc simulations were performed based on HCCI compositions in Table 1 using TCFE8 database. The transition temperatures, particularly the liquidus and solidus temperatures were determined from the calculations, they were then compared to the cooling curves obtained from ATAS thermal analyses. The phases predicted were also compared with those obtained from microscopy.

ATAS thermal analyses were carried out to determine the cooling curves for the different compositions of HCCIs melted in an induction furnace. The simulation was done by pouring molten HCCIs in ATAS quick cups connected to ATAS MetStar software. The dimensions of the ATAS cup are 64.7 mm high, 51.5 mm wide and a wall thickness of approximately 7 mm. In the cup, is a thermocouple, which transmits the temperature of the HCCIs ingot to the software as it, solidifies.

2.2.2 Heat treatment of HCCIs

A destabilisation heat treatment procedure was performed on selected HCCIs to see the effects on microstructure, hardness, and fracture toughness. The heat treatment was carried out at 950 °C for 5 h, then they were quenched in oil. This was done to promote the conversion of austenite to martensite. After quenching, a tempering treatment was performed at 550 °C for 6 h in accordance with [8,10]. Tempering was done to promote the precipitation and growth of secondary carbides. It also reduces residual stresses in the material, ultimately softening it and increasing toughness without compromising the hardness significantly. The samples were then subjected to microstructural examination.

2.2.3 Metallography and microstructural examination

HCCI samples subjected to microstructural examination were prepared following standard metallographic procedures. Sectioned HCCI samples were mounted in a polyfast resin and the surface were subjected to grinding using

different grades of silicon carbide abrasive paper (300−1200 grit) and polishing using 0.25 µm diamond paste. The polished samples were then etched using standard Murakami reagent which was prepared by mixing 10 g of potassium ferricyanide $K_3[Fe\ (CN)_6]$ with 10 g of potassium hydroxide (KOH) and then dissolved in 100 ml distilled water.

The microstructure of the samples was examined using the Olympus GX41 optical microscope and a Zeiss-Sigma field emission gun scanning electron microscopy (FEG-SEM) operated in back scattered electron imaging mode. The micrographs obtained were used to establish the microstructural constituents of the as-cast and heat treated HCCIs. Additionally, the worn surfaces of selected HCCIs subjected to wear testing were examined on FEG-SEM. Stereo microscope was used to evaluate the extent of wear on the alumina ball used during wear test.

2.2.4 Hardness and fracture toughness testing

The Vickers hardness of selected HCCI samples was measured using FM 700 hardness testing machine. Five indentations were randomly made on each surface of the samples using a load of 300 gf and a dwell time of 10 s, the average representative values of hardness were then obtained. Indentations were spaced sufficiently far apart so that the indentation behaviour was not affected by the adjacent indentations. The same load and dwell time was used to measure the hardness of the samples after destabilisation heat treatment and after tempering.

Selected HCCI samples were subjected to 3-point bend test to obtain their ultimate fracturing forces. During testing, samples were placed on top of two supports which had 12.70 mm between them. The third support remained on top (centre) of the sample above the notch. The machine was started, and a pressing force was applied on the sample until it fractures. The results of the ultimate fracturing forces for the as-cast samples were obtained and recorded for later use in calculating their fracture toughness (K_{IC}) following equations (2) and (3) [11].

$$K_Q = \frac{P_Q}{BW^{3/2}} * f\left(\frac{a}{w}\right) \tag{2}$$

and; $f\left(\frac{a}{w}\right)$

$$f\left(\frac{a}{w}\right) = 3\left(\frac{a}{w}\right)^{\frac{1}{2}}\left[1.99 - \left(\frac{a}{w}\right)\left(1 - \frac{a}{w}\right) \times \left(2.15 - 3,93\left(\frac{a}{w}\right) + 2.7\left(\frac{a^2}{w^2}\right)\right]\right] \Big/ 2\left(1 + \frac{2a}{w}\right)\left(1 - \frac{a}{w}\right)^{3/2} \tag{3}$$

where P_Q is the load at which the sample fractures in kN, B is the specimen thickness in cm, a is the crack length in cm, and W is the specimen's depth in cm.

Therefore, the parametric relationships are defined in equations (4)–(6);

$$a = 1\text{mm} \times \frac{0.1\text{cm}}{1\text{mm}} = 0.1\text{cm} \tag{4}$$

Table 2. Parameters used for wear testing.

Parameters	Values
Load	5 N
Temperature	20 °C
Duration	4500 s
Linear speed	0.100 m/s
Ball type	Al_2O_3
Ball radius	3 mm
Sliding distance	450 mm
Humidity	40%

$$B = W = 5\text{mm} \times \frac{0.1\text{cm}}{1\text{mm}} = 0.5\text{cm} \tag{5}$$

$$S = 12.70\text{mm} \times \frac{0.1\text{cm}}{1\text{mm}} = 1.27\text{cm}. \tag{6}$$

All samples had the same crack length, thickness, span, and width. P_Q differs for all the samples.

2.2.5 Wear testing

The dry sliding wear tests were carried out using a ball-on-disc tribometer which operates with linear reciprocating motion drive. A stationary ball of alumina was pressed against a rotating disc holding the HCCI samples for 4500s. The coefficient was measured while the test was still running until it stops. The test parameters that were used are presented in Table 2.

3 Results

3.1 Prediction of microstructural constituents and transition temperatures

Figure 1 shows results from Thermo-Calc analysis on HCCI samples. It can be observed that the dominant phases predicted to be stable at temperatures below 400 °C are M_7C_3 carbides, BCC_A2 ferrite and $M_{23}C_6$ carbide phases. Below the liquidus, both austenite (FCC_A1) and M_7C_3 carbides phases are formed in all samples, but the austenite transformed to BCC_A3 (ferrite) at temperatures below 800 °C. Also, $M_{23}C_6$ also formed from the M_7C_3 carbides at ~730 °C in HCCI samples A and C and ~780 °C in HCCI samples B and D. The number of phases present in all the HCCI samples at 400 °C are quite similar except in sample C where $M_{23}C_6$ phase is higher *i.e.*, ~6% as opposed to ~3% (Fig. 1). This may be due to higher Mo content and lower Cr/C ratio or other alloying elements like, V, Ni, and Co in comparison with HCCI samples A, B and D.

The solidus and liquidus temperatures extracted from the Thermo-Calc curves are presented in Table 3. The solidus for all the HCCI samples was 1300 °C and the liquidus is 1320 °C in all HCCI samples except in HCCI sample C, where the liquidus rose to 1340 °C owing to lower

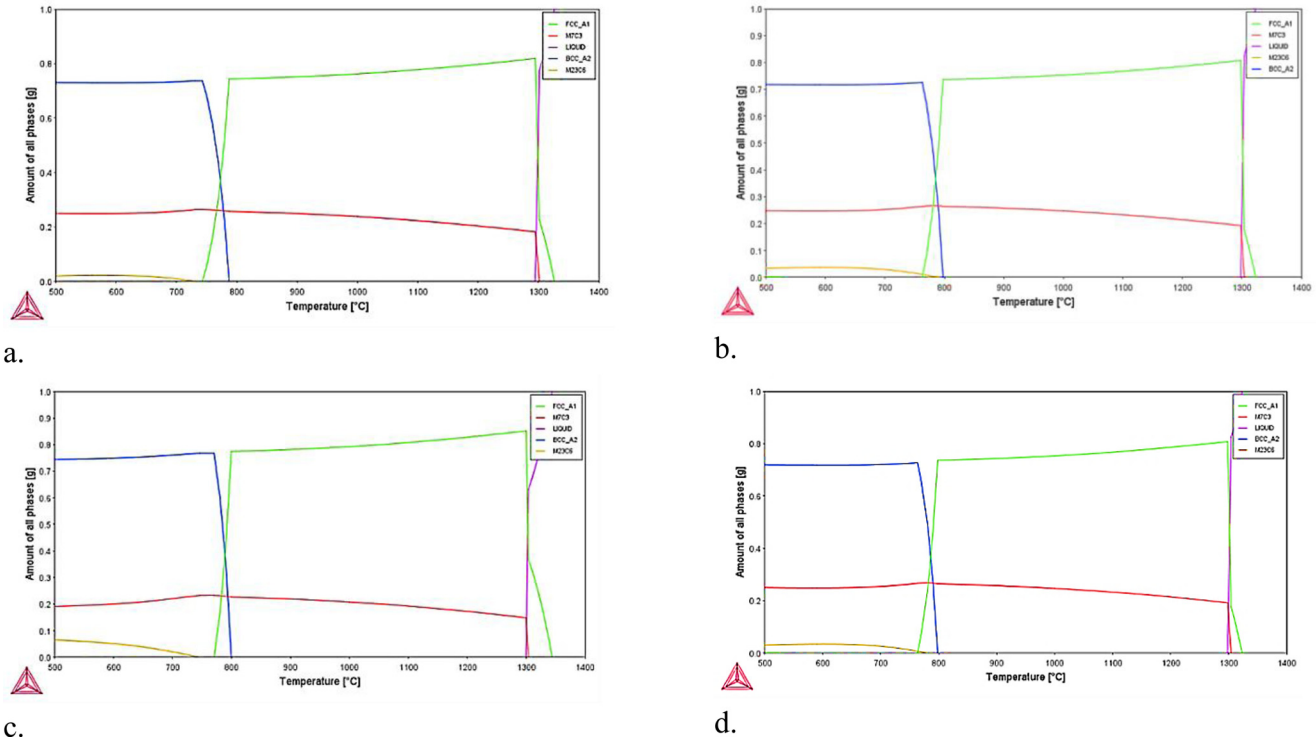

Fig. 1. Phase prediction using TCFE8 database on Thermo-Calc for (a) HCCI A; (b) HCCI B; (c) HCCI C; and (d) HCCI D.

Table 3. Transition temperatures obtained from Thermo-Calc and ATAS Metaster.

	HCCI sample	**Thermo-Calc (TCFE8)**		**ATAS Metaster**
	Liquidus (°C)	Solidus (°C)	Liquidus (°C)	Solidus (°C)
A	1320	1300	1300	1180
B	1320	1300	1280	1200
C	1340	1300	1270	1200
D	1320	1300	1270	1210

carbon content. On the Fe-C phase diagram the liquidus decreased with increasing carbon content up to the eutectic composition.

The transition temperatures obtained from the Thermo-Calc analysis were then compared to those obtained from ATAS thermal analysis cooling curves (Fig. 2). HCCI samples A and B exhibited similar cooling profile with large freezing range in comparison with HCCI samples C and D that both show small freezing rage. In addition, the freezing range in HCCI samples A and B is less steep in comparison with that of HCCI samples C and D, indicating that HCCI samples A and B had slower solidification time than that of HCCI samples C and D. Despite this trend, the liquidus and solidus temperatures extracted from the cooling curves (Tab. 3) show that the values vary considerably in the HCCI samples except the liquidus of HCCI samples C and D and solidus for HCCI samples B and C. When comparing the ATAS results with the Thermo-calc predictions, the liquidus and solidus temperatures are more sensitive to the compositional variations in the HCCI samples. This may be attributed to the non-equilibrium nature of the actual solidification process as opposed to the Thermo-calc predictions that were obtained under equilibrium conditions. Additionally, there are microconstituents such as S, P, B, Sn, Nb, Co and Pb that are found in the compositional analysis which can affect the solidification profile of HCCI but were not considered during the Thermo-Calc simulations.

3.2 Microstructure of as-cast and heat treated HCCI samples

Figure 3 shows the optical images of HCCI samples with different compositions. Selected SEM images of HCCI A and HCCI B are also shown in Figure 4. The alloys consist of dendritic austenite surrounded by carbides of either M_7C_3 and/or $M_{23}C_6$. According to the Thermo-calc results, ferrite phase, M_7C_3 carbides and $M_{23}C_6$ carbides are expected in the microstructure of the HCCI samples under equilibrium condition (Fig. 1), but due to faster solidification rate of the HCCI samples, dendritic austenite is retained in the microstructure of the HCCI samples. It is possible that traces of $M_{23}C_6$ carbides or other carbide types can be found in the alloys, but this will require

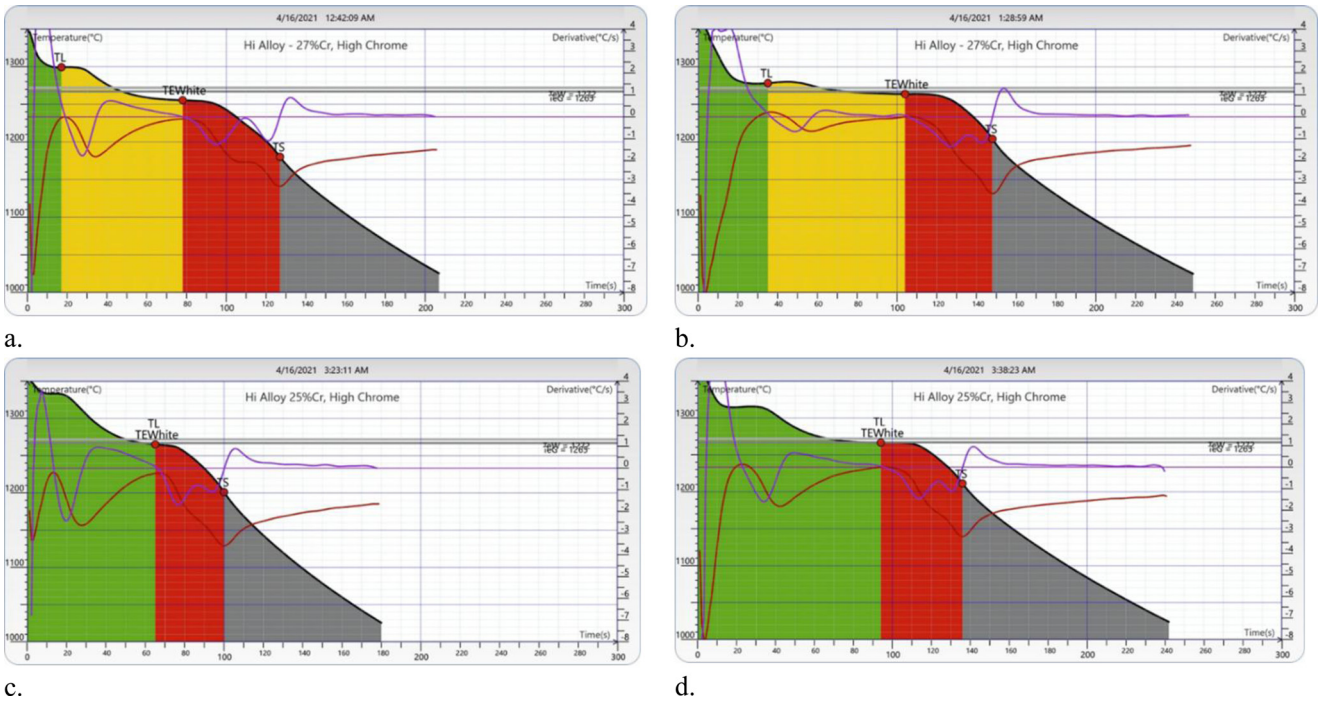

Fig. 2. Cooling curve obtained from ATAS Metaster for (a) HCCI A; (b) HCCI B; (c) HCCI C; and (d) HCCI D.

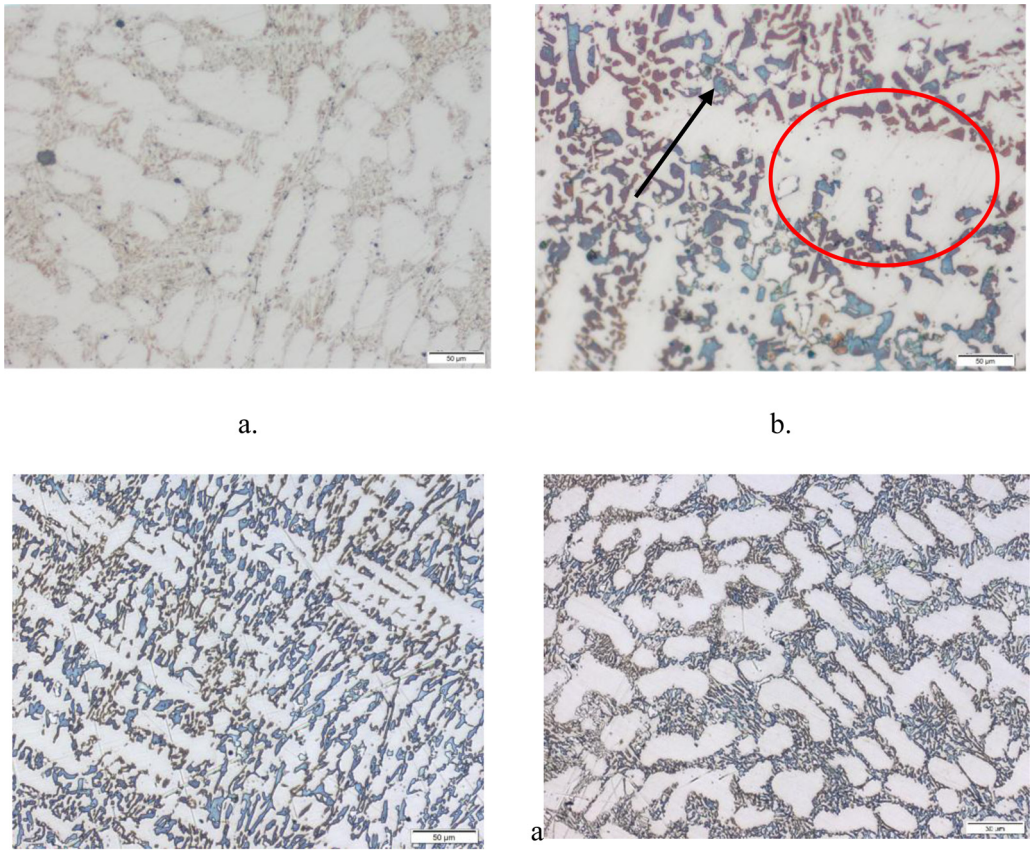

Fig. 3. Optical micrograph of select as-cast samples (a) HCCI A; (b) HCCI B; and (c) HCCI C; and (d) HCCI D.

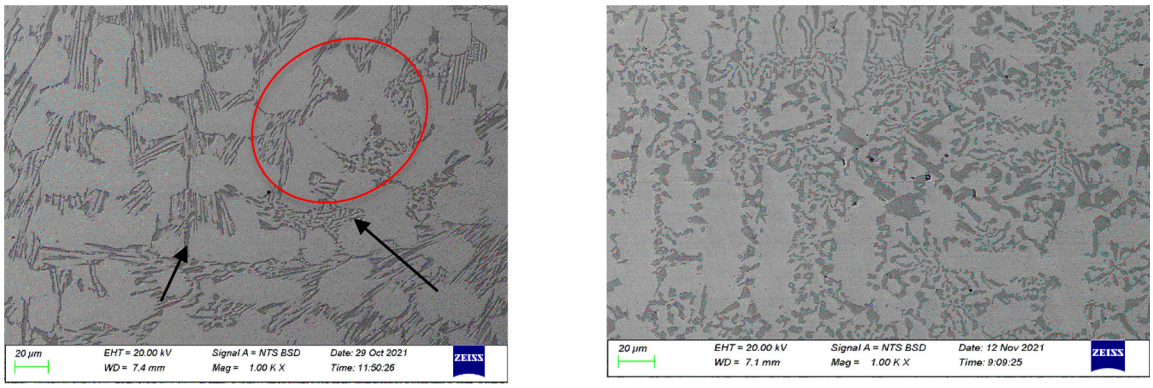

Fig. 4. SEM images of selected samples (a) HCCI A and (b) HCCI B. Red circle indicates the dendritic austenite while the black arrows show the M_7C_3 and/or $M_{23}C_6$ carbides.

additional characterisation such as transmission electron microscopy and X-ray diffraction which are not considered in this work. The austenite dendrites in HCCI A and HCCI B are coarser than that of HCCI C and HCCI D. This agrees with the ATAS cooling curves presented in Figure 2, both HCCI A and HCCI B have longer solidification time which means that the solidification rate was slower in comparison with HCCI C and HCCI D, thus leading to coarse austenite dendrites in the alloys.

Figure 5 shows the optical micrographs of HCCI samples after quenching and tempering treatments. For all the samples, the quenching and tempering treatments refined the microstructures when compared to the as-cast microstructures. No significant change is observed between as quenched and as-tempered microstructures for all the alloys except in HCCI D where the tempered microstructure shows coarser austenite grains and dissolution of carbide phase in comparison with the as-cast and as-quenched sample. The dendritic features in the tempered HCCI D samples are less prominent.

It is expected that the stress induced by quenching should be reduced as a result of tempering treatment. Therefore, increased hardness is expected in the quenched HCCI samples while improved toughness is expected in the tempered HCCI samples. This will be confirmed in Section 3.3.

3.3 Mechanical properties of HCCI

3.3.1 Hardness

Table 4 shows the hardness of HCCI samples under different conditions. The hardness of the alloys differs with varying composition as indicated by the Cr/C ratio. Additionally, the quenching treatment increased the hardness of the HCCI alloys significantly owing to grain refinement and possible austenite to martensite transformation on quenching. After tempering treatment, the hardness of all the HCCI samples decreased significantly and was lower than the hardness of the as-cast alloys except in HCCI B where the hardness of the as-cast and tempered condition are similar. The reduction in hardness may be attributed to stress-relief effect of the tempering process or possible transformation of martensite to ferrite.

3.3.2 Fracture toughness

The ultimate forces and calculated fracture toughness of the HCCI samples in both as-cast and tempered conditions are presented in Table 5. The K_Q values increased after the samples have been tempered in all the samples except HCCI B where it decreased. This again show that slight compositional variation has effect on the properties of the HCCI alloys. The Cr/C ration in HCCI B is approximately 11 while it is approximately 10 for the remaining alloys. The response of the alloys to tempering treatment in terms of fracture toughness is optimum as Cr/C approaches 10. When Cr/C ratio is less than 10, only a marginal increase in K_Q is observed, but when Cr/C exceeds 10 the KQ reduced significantly. Since there is a linear relationship between K_Q and K_{IC}, the toughness of the alloy increases once K_Q has been proven to be equal to K_{IC}. A ratio of $2.5\left(\frac{KQ}{\sigma ys}\right)^2$ for most alloys has been proven to be greater than both the thickness (B) and the crack length (a) of the alloys and thus K_Q equating to K_{IC}.

3.4 Wear

Figure 6 shows the evolution of coefficient of friction versus the test duration for HCCI A, HCCI C and HCCI D samples subjected to wear test. HCCI B was not considered since its fracture toughness degraded after tempering. It is observed that the coefficient of friction is generally lower in HCCI D when compared with HCCI A and HCCI D. This shows that despite the similar Cr/C ratio in the alloys, the wear behaviour of HCCI samples differ. HCCI D with the highest V content and highest fracture toughness after tempering had best wear behaviour.

The width of the wear track of each HCCI samples was measured by measuring the width of the wear track at the top, bottom, on the left and on the right as shown in Figure 7.

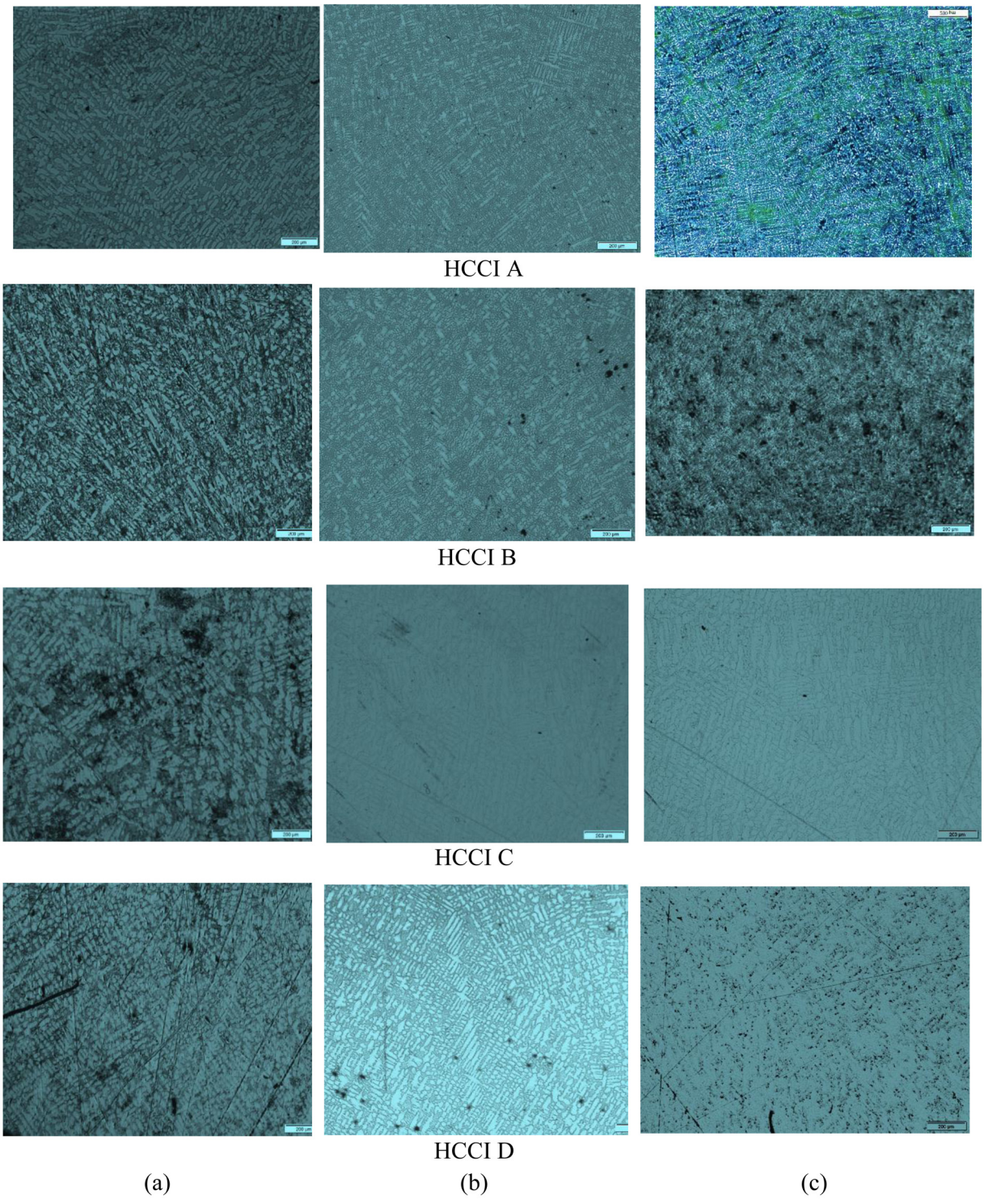

Fig. 5. Optical micrograph of HCCI samples in different conditions (a) as-cast; (b) destabilisation heat treatment; and (c) tempering.

The wear widths are presented in Table 6. It is observed that the width of the wear track is more consistent in HCCI C compared to HCCI A and HCCI D. It can also be seen that HCCI D has small widths compared to HCCI A and HCCI C.

After the test was performed for each sample, visual inspection of the wear on the ball was carried out using a stereoscopic microscopy device. The wear on the ball for HCCI D is significantly small (Fig. 8), hence it has a small width on all measured positions in comparison with HCCI A and HCCI C.

Table 4. Hardness of selected HCCIs in as cast and heat-treated conditions.

HCCI sample	Cr/C	As-cast (HV)	After destabilisation heat-treatment (HV)	After tempering (HV)
HCCI A	10.00	545 ± 14	745 ± 11	532 ± 38
HCCI B	10.80	535 ± 15	769 ± 32	539 ± 15
HCCI C	9.59	435 ± 7	673 ± 21	413 ± 7
HCCI D	9.95	465 ± 13	694 ± 16	424 ± 8

Table 5. Ultimate force and fracture toughness of HCCI samples.

HCCI samples	**Force (N) in as-cast condition**	**Force (N) in tempered condition**	**KQ ($MPa \cdot m^{0.5}$), as-cast**	**KQ ($MPa \cdot m^{0.5}$), tempered**
HCCI A	3247.87	4451.61	38.769	53.138
HCCI B	4287.48	3168.46	51.178	37.821
HCCI C	3573.15	3928.24	42.652	46.890
HCCI D	3663.54	4652.80	43.730	55.539

Figure 9 shows the wear scar on the HCCI samples. As expected, the wear scar on HCCI D is smaller than that of HCCI A and HCCI C, indicating the superior wear resistance of HCCI D over HCCI A and HCCI C.

4 Discussion

In many jobbing foundries, compositional analysis has remained a prominent quality control criterion for assessing the acceptability of cast components. The targeted compositions are specified as a range between minimum and maximum permissible limits of critical alloying elements. For example, in this work, the targeted compositions for the HCCI samples are presented in Table 7. It would be expected that any composition that fall within the specified range should have similar microstructural features and properties. The HCCI samples in this work fall within the compositional limits presented in Table 7. However, our results show the compositional variations in the HCCI samples affect the microstructure and properties of the alloys.

From microstructural point of view, it is expected that under equilibrium conditions, all the HCCI samples are expected to have similar microstructural constituents – ferrite and M_7C_3 or $M_{23}C_6$ carbides (Fig. 1), since their compositions fall within the targeted compositional band. This is further corroborated by the similar solidus and liquidus temperatures predicted for most of the alloys (Tab. 2). However, faster cooling rate during solidification led to the stabilisation of the austenite phase at ambient temperature as opposed to the ferrite phase predicted by Thermo-Calc. Also, the solidus and liquidus obtained from cooling curve showed more variations in response to the different compositions of the HCCI samples. This confirm that cooling rate under solidification conditions are typically faster than cooling rate under equilibrium conditions. There have been contradicting views on the role of Mo on the structural evolution of HCCI. Imurai et al. [12] and Scandian et al. [13] reported that Mo addition promote the formation of $M_{23}C6$ and M_6C carbides, Ikedia et al. [14] reported that adding 1 wt.% Mo to HCCI formed M_2C phase, but Dupin et al. [15] reported that adding 1 wt.% Mo to HCCI with Cr/C ratio7 did not change the microstructure. In this work, Mo content was below 1 wt.%, hence Mo induced carbides are not expected. While it could not be established whether $M_{23}C_6$ carbide is present in the as cast HCCI samples, the microstructures already show that the two dominant phases are austenite and M_7C_3 carbides. This is consistent with previous studies [8, 9,16] where dendritic austenite and M_7C_3 carbides have been reported for similar composition range. High Cr/C ratio and the inclusion of Mo, Ni and Cu have also been reported to prevent formation of ferrite or pearlitic phase in HCCIs, favouring austenite formation.

It would be expected that since the composition of the four HCCI samples fall within the targeted band, the cooling curves should be similar. However, the cooling curves differ, and it is not very clear how this is influenced by the composition of the HCCI samples. The freezing range and the steepness of the cooling curves clearly had influence on the size of the dendritic austenite (Fig. 2), but there is need for further investigation on how this may have been influenced by the difference in composition of the alloys. It is believed that this understanding may help in controlling the grain size of HCCI alloys.

Heat treatment has been applied to HCCI to manipulate the microstructure and properties particularly
hardness and wear [17,18]. The morphology and crystallographic properties of constituent phases, proportion of martensite, retained austenite and carbides are all the important factors influenced by heat treatment [17–20]. In this study, the microstructure of

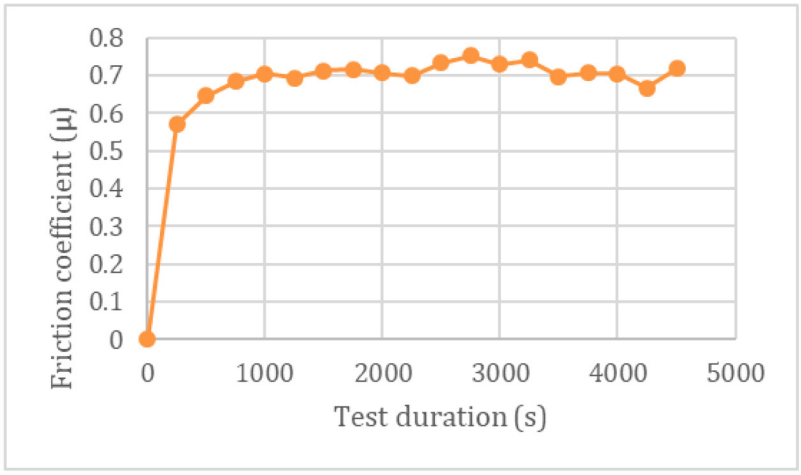

(a)

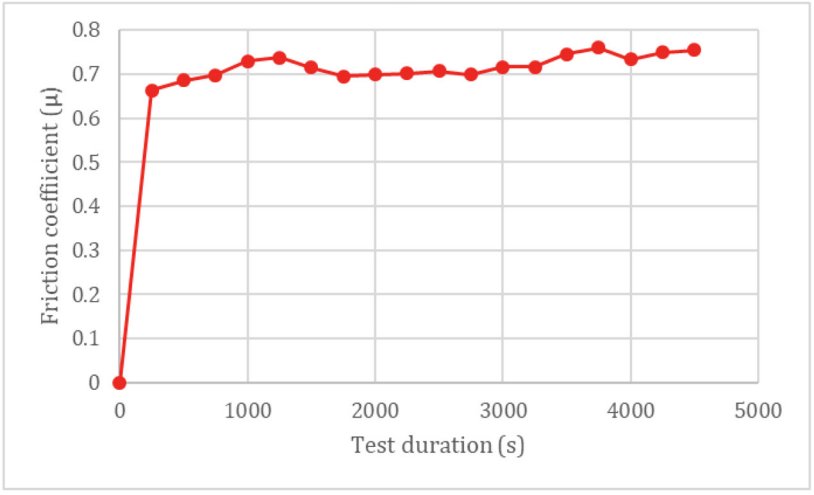

(b)

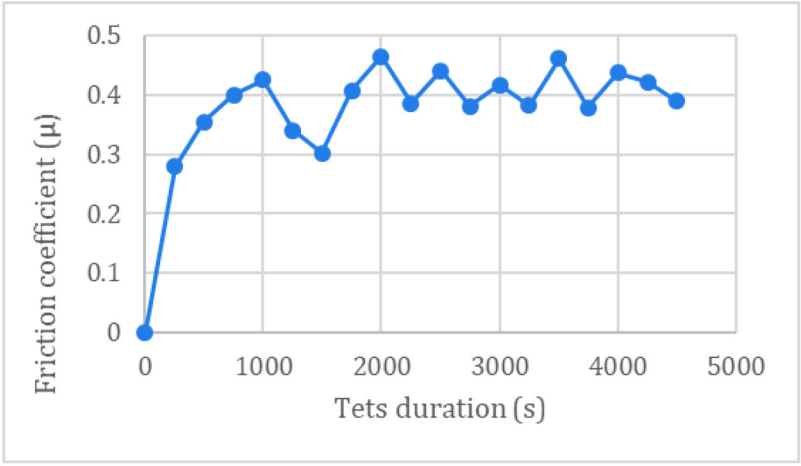

(c)

Fig. 6. Coefficient of friction versus time for (a) HCCI A (b) HCCI C; and (c) HCCI D.

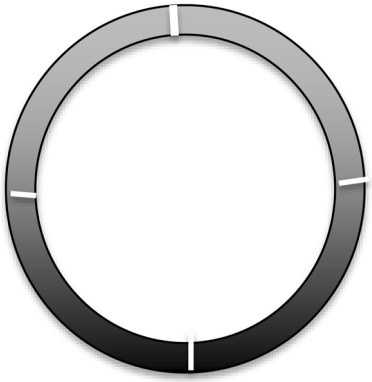

Fig. 7. The location of the profile measurements along the wear track.

the HCCI alloys got refined after quenching. No significant change was observed in the microstructure after tempering except in HCCI D which showed significant change in the size and morphology of the austenite phase. The lower resolution of the optical micrographs made it impossible to really establish the microstructural changes that may have occurred in the HCCI. Previous authors have reported that stabilisation treatment caused formation of martensite and other secondary carbides which increased the hardness and wear resistance of HCCI alloys [8,9].

From the hardness, fracture toughness and wear results, the influence of compositional variation is more conspicuous. It would be expected that with the composition of all the HCCI samples falling within the targeted compositional limit, the hardness of the HCCI samples should be close. However, the hardness result under different conditions – as cast, as-quenched and as-tempered did show dependence of compositional variation. Previous researchers [8,9] have shown that increasing carbon, chromium, vanadium contents increase the hardness of HCCIs alloys, while increasing Si content decrease the hardness of HCCI alloys. In this work, the amount of Si, V, Ni, Cu and Mo are mostly <1 wt.% and may not necessarily influence the hardness of the HCCI samples. Also, increasing chromium content, carbon content, Cr/C ratio or total carbide volume cannot be directly correlated with the hardness of the HCCI samples. However, it is observed that HCCI A and B had superior hardness in the as-cast, quenched and tempered conditions in comparison with HCCI C and D. This follows similar trend as that of the cooling curve in relation to the austenite grain size. It is interesting to note that HCCI A and B with larger dendritic austenite grains are harder than HCCI D. This suggests that there may be precipitation of harder secondary phases within the grains of the austenitic dendrite that is responsible for this trend. Therefore, further characterisation of the microstructural constituents of HCCI A and B relative to HCCI C and D would help clarify the effect of compositional variation on the observed hardness.

There has been recent interest in improving the fracture toughness of HCCI by some researchers. This is aimed at enhancing the in-service performance of HCCI components since they are very brittle. It was reported that adding 1.5–3 wt.% vanadium to HCCI refine the microstructure and improved the fracture toughness. In this work, vanadium content in all the HCCI samples was less than 1.5 wt.% [6]. Hence, vanadium induced grain refinement or improved fracture toughness may not be expected. The fracture toughness of the HCCI samples show sensitivity to the variations in compositions and tempering treatment. In the as-cast condition, fracture toughness was highest in HCCI B but after tempering the fracture toughness degraded significantly. The remaining HCCI samples showed improved fracture toughness after tempering. This may be attributed to spheroidization of the M_7C_3 carbides or the evolution of tempered martensite, pearlite and soft ferrite-$M_{23}C_6$ precipitates [8]. One would expect that since all the HCCI samples had compositions that are within the targeted limits, the fracture toughness in the as-cast and heat treatment conditions be comparable. However, the fracture toughness differed with composition as well as heat treatment. The wear results also follow similar trend as fracture toughness, the three selected HCCI samples displayed different coefficient of friction and the wear volume vary significantly. This depicts that compositional changes affect the performance of HCCI components in service.

Table 6. Representative wear width of alumina ball used on selected HCCI samples.

HCCI samples	Wear width (μm)			
Top	Bottom	Left	Bottom	
HCCI A	373	338	327	370
HCCI C	294	294	279	300
HCCI D	251	255	283	293

The use of targeted compositional limits for assessing the quality of cast HCCI require a more stringent analyses because the failure of HCCI components in service may be attributed to compositional variations in components which are accepted because their compositions fall within the targeted compositional limits. From the results shown in this study, despite the compositional variations in the HCCI samples, the cooling curve from ATAS simulation seem to have shown more consistency in terms of the agreement between the cooling profile, microstructure, and hardness. However, more work is needed to establish the correlation between composition and cooling profile of HCCI alloys. This will be a necessary step in determining a more stringent compositional limits for reproducible properties in HCCI.

5 Conclusion

The use of compositional analysis alone to qualify acceptable HCCI castings in jobbing foundries is a common practice. The targeted composition of accepted components for industrial use is usually specified within a range. Therefore, in practice, the amount of constituent elements in high chrome cast iron can vary slightly without

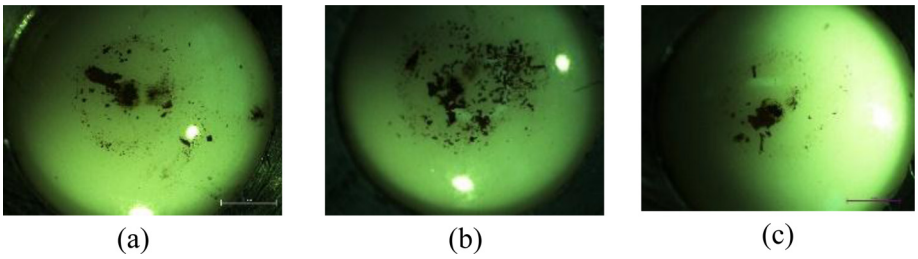

Fig. 8. Stereo image showing wear on alumina ball for (a) HCCI A; (b) HCCI C; and (c) HCCI D.

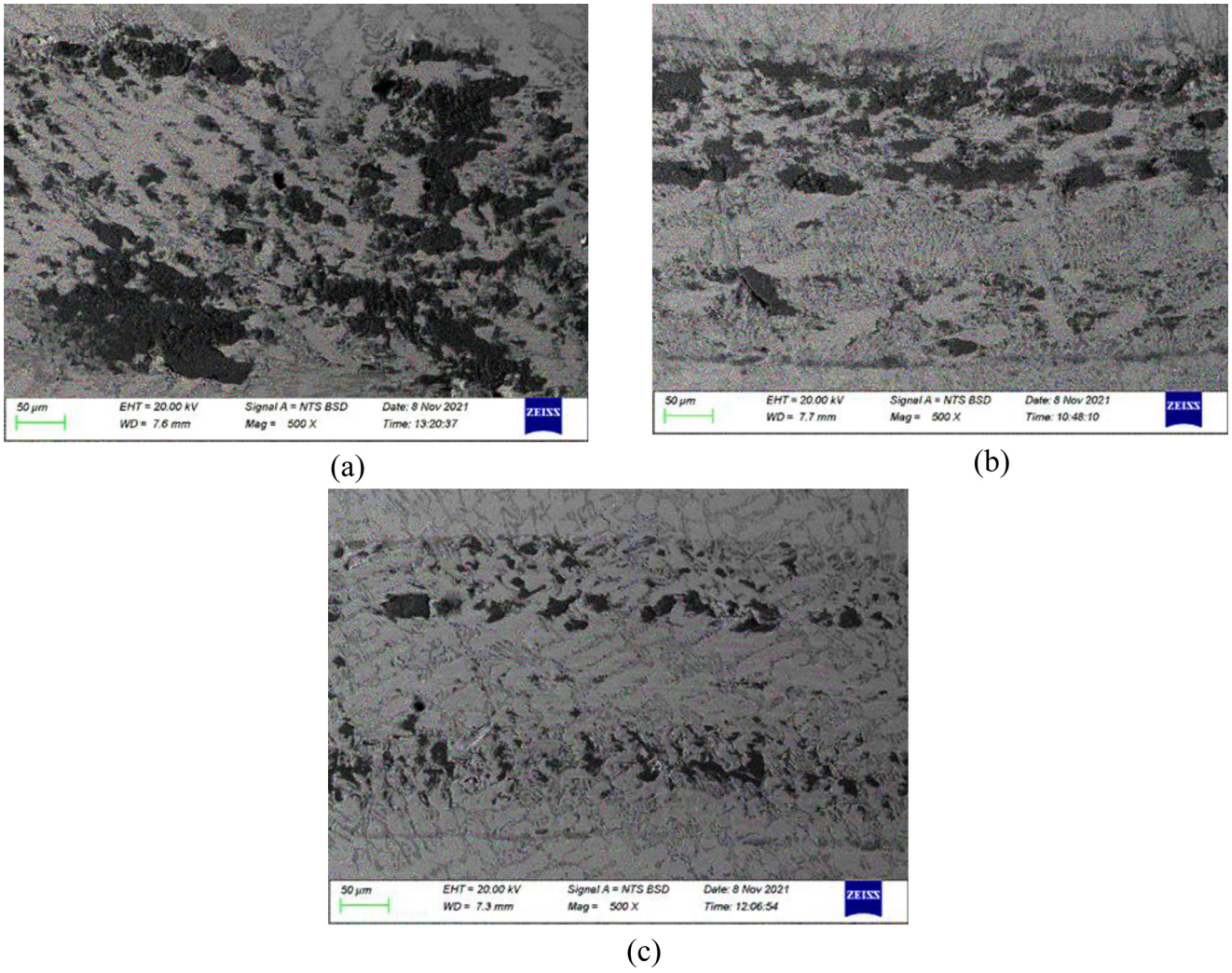

Fig. 9. SEM image of wear scar on (a) HCCI A; (b) HCCI C; and (c) HCCI D.

Table 7. Targeted composition of HCCI samples.

Elements	C	Cr	Si	Mn	Ni	Cu	Mo	V
Min	22	2	0.5	0.5	–	–	–	–
Max	28	2.8	1	1.5	0.5	0.5	1.5	–

exceeding the targeted compositional range. In this work, we demonstrated that even slight compositional variations can significantly affect the microstructure, hardness, and wear performance of high chrome cast iron. Consequently, more stringent acceptance criteria must be developed for quality control in jobbing foundries. Although further studies are required to achieve this, it can be deduced from this study that exploring the potential of thermal analyses for obtaining solidification profiles appears to be one of the promising approaches to consider for both microstructural control and reproducible mechanical properties of high chrome cast iron components.

Acknowledgements

The authors acknowledge the funding from National Research Foundation (NRF), University of Johannesburg, South Africa in support of the research that produced this work. The authors appreciate the contributions of Willy Chabalalala, Nhlakanipho Sithebe, Marema Khuduwe and Michael Bodunrin for their assistance on the different aspects of the experiment.

References

1. Calmet, Different types of Cast Iron, 2017. http://www.calmet.com/different-types-of-cast-iron/ (accessed July 15, 2021)
2. M.E. Maja, M.G. Maruma, L.A. Mampuru, S.J. Moema, Effect of niobium on the solidification structure and properties of hypoeutectic high-chromium white cast iron, J. South. Afr. Inst. Min. Metall. **116** (2016) 981–985
3. R. Singh, Mechanical properties and testing of metals, in R. Singh (Ed.), Applied Welding Engineering 3rd edn. Butterworth-Heinemann, Oxford, United Kingdom, 2020, pp. 97–104
4. A.K. Patwardhan, A.K. Gupta, N.C. Jain, M.N. Saxena, Failure Investigation of Cast-Iron Spun Pipes- A Case Study(Retroactive Coverage), Tool Alloy Steels **18** (1984) 309–312
5. M. Ngqase, X. Pan, An overview on types of white cast irons and high chromium white cast irons, J. Phys. Conf. Ser. **1495** (2020) 1–11
6. L.A. Mampuru, M.G. Maruma, J.S. Moema, Grain refinement of 25 wt.% high chromium white cast iron by addition, J. South. Afr. Inst. Min. Metall. **116** (2016) 969–972
7. A.B. Jacuinde, B. Hernandez, L.B. Gomez, SEM study on the M7C3 carbide nucleation during eutectic solidification of high-chromium white irons, Z. Met. kd. **12** (2005) 1380–1385
8. K. Abdel-Aziz, M. El-Shennawy, A.A. Omar, Microstructural characteristics and mechanical properties of heat treated high-Cr white cast iron, Int. J. Appl. Eng. Res. **12** (2017) 4675–4686
9. E. Karantnzalis, A. Lekatou, H. Mavros, Microstructure and properties of high cast irons: effect of heat treatment and alloying additions, Int. J. Cast Met. Res. **22** (2013) 448–456
10. G.E. Dieter, in *Mechanical Metallurgy*. Createspace Independent Publishing Platform (2012)
11. ASTM, Standard Test Methods Plane-Strain Fracture Toughness and Strain Energy Release Rate of Plastic Materials. ASTM International (2007)
12. S. Imurai, C. Thanachayanont, J.T.H. Pearce, K. Tsunda, T. Chairuangsri, Effects of Mo on microstructure of as-cast 28wt.% Cr-2.6wt. %C-(0-10) wt.% Mo irons, Mater. Charact. **90** (2014) 99–112
13. C. Scandian, C. Boher, J.D.B. de Mello, F. Rezai-Aria, Effect of molybdenum and chromium contents in sliding wear of high-chromium white cast iron: the relationship between microstructure and wear, Wear **267** (2009) 401–408
14. M. Ikedia, T. Umeda, C.P. Tong, T. Suzuki, N. Niwa, O. Kato, Effect of molybdenum addition on solidification structure, mechanical properties and wear resistivity of high chromium cast irons, ISIJ Int. **32** (1992) 1157–1162
15. P. Dupin, J.M. Schissler, Influence of addition of silicon, molybdenum, vanadium and tungsten upon the structural evolution of the as-cast state of a high-chromium cast iron (20% Cr, 2.6%C), AFS Trans. **92** (1984) 335–360
16. M. Salasi, G.B. Stachowaik, G.W. Stachowaik, Three-body tribocorrosion of high chromium cast irons in neutral and alkaline environments, Wear **271** (2011) 1385–1396
17. A. González-Pociño, F. Alvarez-Antolin, J. Asensio-Lozano, The joint effects of nitriding and parameters related to the destabilisation of austenite on wear resistance in white cast iron with 25% cr. Metals **11** (2021) 85
18. S. Zhou, Y. Shen, H. Zhang, D. Chen, Heat treatment effect on microstructure, hardness and wear resistance of Cr26 white cast iron, J. Chin. Soc. Mech. Eng. Trans. Chin. Inst. Eng. **28** (2015) 140–147
19. G. Hakan, E. Faith, Effects of destabilization heat treatment on the microstructure and abrasive wear behaviour of high-chromium white cast iron investigated using different characterization techniques, Metall. Mater. Trans. A **44A** (2013) 4993
20. M. Ngqase, X. Pan, XRD investigation on heat treatment of high chrome white cast irons, J. Phys. Conf. Ser. **1495** (2020) 1495

Cite this article as: Brayner Ndivhuwo Nelwalani, Josias van der Merwe, Vhonani Munyangane, Zaynab Adam Cader, Thato Rampaku, Desmond Klenam, On the influence of compositional variations in high chrome cast iron: an assessment of microstructure and mechanical behaviour, Manufacturing Rev. **11**, 9 (2024)